The International Journal of Advanced Manufacturing Technology (2021) 113:159–176
https://doi.org/10.1007/s00170-020-06519-9

ORIGINAL ARTICLE

Modelling and interaction analysis of the self-pierce riveting process using regression analysis and FEA

Huan Zhao[1] · Li Han[2] · Yunpeng Liu[1] · Xianping Liu[1]

Received: 17 August 2020 / Accepted: 15 December 2020 / Published online: 21 January 2021

Abstract
Self-pierce riveting (SPR) is a major joining method used in the automotive industry. However, there still lacks a fast and easy-to-use joint quality prediction tool available for the automotive engineers. In this study, the simple but effective regression analysis method was applied to quickly predict the SPR joint quality. Two regression models were developed for the prediction of the interlock and the minimum remaining bottom sheet thickness (T_{min}). The prediction accuracy of the developed regression models was validated by comparing with the experimental results. Under the studied joint configurations, the mean absolute errors (MAE) of the interlock and T_{min} were 0.047 mm and 0.053 mm, respectively, and the corresponding mean absolute percentage errors (MAPE) were 10.4% and 12.3%. With the developed models, the interaction effects between rivet and die parameters on the joint interlock and T_{min} were also systematically analysed. The results revealed that the rivet and die parameters demonstrated significant influences on the interlock but not on the T_{min}. These interaction effects were further examined by analysing the deformations of the rivet and substrate materials. Moreover, the die-to-rivet volume ratio (R) was found to be critical for the formation of interlock, and a larger interlock is more likely achieved when the R is close to 1.0.

Keywords SPR · Multiple regression model · Interaction effect · Rivet length · Die geometry · Die-to-rivet volume ratio

1 Introduction

With the increasing applications of lightweight materials, especially aluminium alloys, in body-in-white (BIW) structures, self-pierce riveting (SPR) has become one of the major connection methods in the automotive industry [1]. As a mechanical joining approach, SPR is capable of connecting two or more layers of similar or dissimilar materials, such as aluminium alloys, magnesium alloys, steels and even composite materials. It can also be applied on parts with coated or painted surfaces and does not require pre-drilled holes [2–5]. Moreover, the SPR joining system is very convenient to be integrated into the automation production line. Therefore, the SPR technique has been heavily utilized in the automotive aluminium BIW assembly [6, 7].

✉ Xianping Liu
X.Liu@warwick.ac.uk

[1] School of Engineering, University of Warwick, Coventry CV4 7AL, UK

[2] Hansher Consulting Ltd., Coventry, UK

Taking a two-layer joint as an example, the four steps during SPR process are schematically shown in Fig. 1. First, the blank holder moves downward and clamps the two sheets together. Then, the punch moves downward and presses the rivet into the sheets. The rivet shank first pierces through the top sheet and then flares into the bottom sheet. Finally, the punch and blank holder are lifted, and an SPR joint with a mechanical interlock is formed. As shown in Fig. 2, the SPR joint quality is usually assessed by three critical indicators measured on the joint cross-sectional profile: (1) the interlock; (2) the minimum remaining bottom sheet thickness (T_{min}); and (3) the rivet head height [8]. The interlock is critical for the mechanical strengths and failure behaviours of SPR joints. Too small interlock values may result in pull-out failure of the rivet shank from the bottom sheet [9]. The T_{min} is very important for the corrosion resistance and waterproof performance of SPR joints. If the T_{min} was 0.0 or negative, moisture or water invasion would inevitably occur in service. This will accelerate corrosion between the steel rivet and the aluminium sheets and result in premature corrosion failure of SPR joints. Zhang et al. [10] also reported that fatigue failure may occur on the bottom sheet if the T_{min} was very small. The rivet head height not only influences cosmetic appearance of the

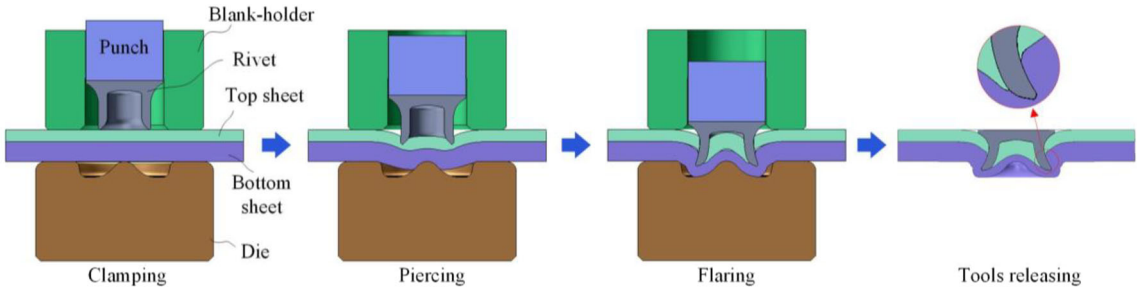

Fig. 1 Schematic of the self-pierce riveting process

connected structure but also the joint corrosion resistance. A protruded rivet head usually causes gaps between the rivet and the connected sheets and thus increases the moisture or water invasion problem. The rivet head height also directly links with the final position of the rivet inserted into the sheets and thus affects the final values of the interlock and T_{min} [11]. The assessment criteria for these three indicators are generally determined by the application requirements of each company and may vary in different industry sectors. For example, according to the standard of a world-leading car manufacturer [6], the interlock should be greater than 0.4 mm for joints with aluminium alloy bottom sheet and greater than 0.2 mm with a steel bottom sheet. The T_{min} should be always greater than 0.2 mm, and fracture of the bottom sheet should be avoided. The rivet head height should be between 0.3 and − 0.5 mm to achieve a smooth surface.

The SPR joint quality can be affected by many parameters, such as the sheet properties, the rivet geometry, the die profile and even the riveting speed [8, 12]. For a given material combination, the selection of rivet and die is most critical for the final SPR joint quality. Many researches were carried out using experimental approach to investigate the influences of rivet and die parameters on the joint quality. For example, Xu [13] experimentally analysed the influences of the rivet length and the die geometry on the interlock and the remaining bottom sheet thickness of AA5754 SPR joints. Similarly, Ma et al. [14] investigated the effects of the rivet length and hardness, the die diameter and pip height on the rivetability of SPR joints with AA6061-T6 and mild steel CR4 sheets. Li et al. [15] evaluated the influences of the rivet tip geometry on the formation of the interlock and the T_{min} in AA5754 SPR joints. However, most of these studies focused on single-factor effects of rivet or die parameters on the SPR joint quality. In fact, during the riveting process, the rivet properties and die profile work together to affect the deformation behaviours of the rivet and sheets. Therefore, the rivet and die parameters would inevitably impose interaction effects on the final joint quality. To deepen understanding of the SPR process and facilitate the rivet and die selection, it is necessary to find out how such interaction effects affect the joint quality. Although the experimental method is a traditional and reliable approach for the study of SPR, it is not a good option to explore the interaction effects considering the heavy investments (e.g. materials, equipment and labour) and long testing time for a huge number of SPR joints.

Over the last few years, many finite element analysis (FEA) models of SPR process have been developed to predict the joint quality and assess the influences of joining parameters on the joint quality. For instance, Mucha [16] developed a two-dimensional (2D) axisymmetric SPR model in MSC Marc Mentat and numerically evaluated the effects of the rivet material properties and the die geometries on the joint interlock and T_{min}. Han et al. [17] numerically studied the main effects of nine independent die parameters on the interlock and the bottom sheet thickness of SPR joints with the DEFORM-2D. Jäckel et al. [18] also numerically studied the influences of five die geometrical parameters on the joint quality. FEA models are much faster than experimental SPR tests. Thus, many vehicle manufacturers gradually apply such FEA models to assist the rivet and die selection for new joints.

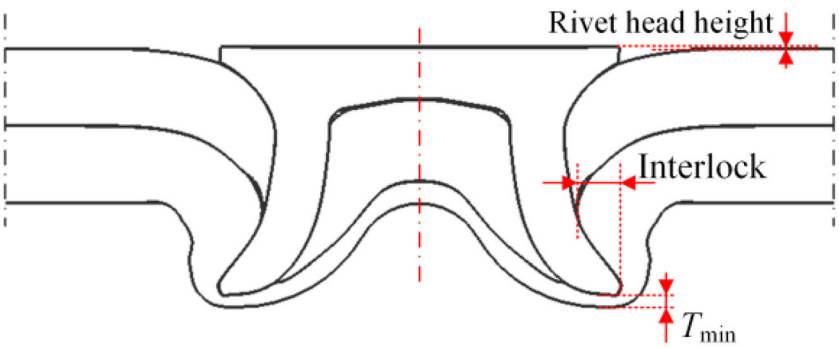

Fig. 2 Quality evaluation indicators of the SPR joint

However, for general engineers without an in-depth knowledge of SPR process and FEA, running such simulation model is still a challenge and it is not easy to identify a suitable rivet and die combination. Meanwhile, the FEA model cannot provide a straightforward result to demonstrate the interaction effects between rivet and die parameters on the joint quality. Therefore, it would be a great contribution for the car industry if a fast and easy-to-use tool could be developed to predict the joint quality and to illustrate the interaction effects between the rivet and die parameters.

The regression model is a simple but effective approach to describe the relationships between independent and dependent variables. It has already been widely applied in many different industrial fields to solve real problems. For example, Bhushan [19] proposed second-order regression models to study the cutting parameters' influences during the turning of aluminium alloy 7075. The power consumption and tool life were also successfully optimized by analysing the corresponding contour graphs. Singh and Ahuja [20] developed regressions models to study the influences of two swellable polymers on the bioadhesive strength and release pattern of the drug. Anawa and Olabi [21] successfully predicted the welding pool geometry of the CO_2 continuous laser welded joints using the proposed multiple regression models. Bitondo et al. [22] also proved the effectiveness of multiple regression models in predictions of welding force and mechanical strength of friction stir welded aluminium joints. Zhao et al. [23] developed a stepwise regression model to predict the nugget diameter of the resistant spot welded DP600 joint with three welding parameters. Unlike the FEA simulation model, the regression model could also be used to easily visualize the interaction effects between different input variables on the target outputs by drawing contour graphs [21–23]. To the authors' knowledge, there are few reports on the applications of regression model or other type mathematic models in quality prediction of SPR joints.

Therefore, this study aims to develop easy-to-use regression models as an alternative to FEA model for SPR joint quality prediction and reveal the interaction effects between the rivet and die. The advantages of the FEA simulation model and orthogonal experimental design were taken to facilitate the development of the regression models and the investigation on the interaction effects. The multiple regression models were developed individually for the interlock and the T_{min} to achieve a high prediction accuracy for each quality indicator. Experimental SPR tests were also carried out to validate the performances of the proposed models. Moreover, interaction effects between the rivet length, die depth and die diameter on SPR joint quality were systematically analysed with corresponding contour graphs drawn from the developed regression models. The importance of the die-to-rivet volume ration (R) on the interaction effects was also highlighted.

2 Joint quality data acquisition

Before developing the mathematical prediction models, the necessary joint quality data under varying joining parameters, including the rivet length (L_1), die diameter (D_1) and depth (H_1), were collected using the developed and verified FEA model. The orthogonal design method was also employed to reduce the total number of simulations.

2.1 FEA model of the SPR process

2.1.1 Model description

The software Simufact. Forming 15, which is mainly designed for simulations of metal forming processes (e.g. forging, clinching and riveting), was adopted in this study to build up the simulation model. Figure 3 shows the developed 2D thermal-mechanical model of the SPR process. The bottom of die was fixed, while the sheet edges could move freely. A 5.3 kN clamping force (F_1) was applied on top surface of the blank holder to clamp the two sheets together. The punch moved downward with a constant speed (v_1 = 100 mm/s) to press the rivet into the sheets. During the riveting process, the punch, blank holder and die undergo very limited elastic deformation and thus were modelled as rigid bodies. While the

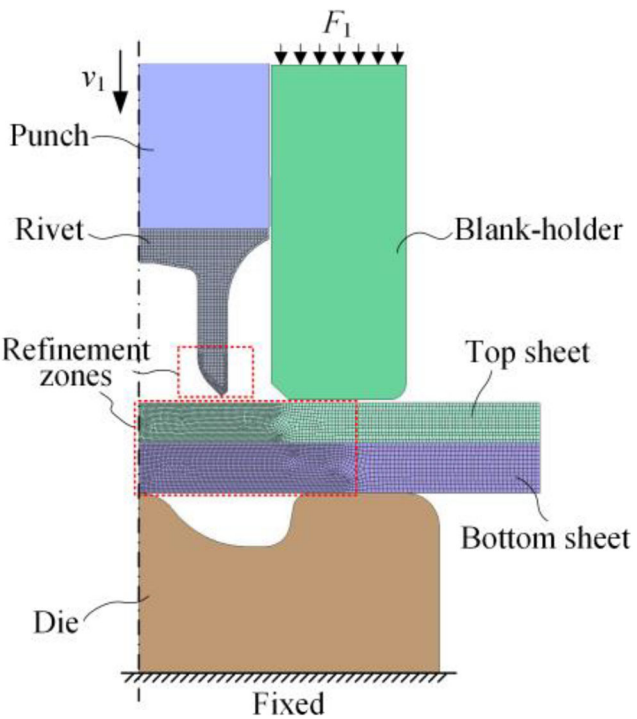

Fig. 3 Schematic of the FEA simulation model

Table 1 Mechanical properties of the rivet [24] and sheet materials [5]

Material	Young's modulus (GPa)	Poisson's ratio	Elongation (%)	Thermal expansion coefficient (1/°C)
AA5754	70	0.33	22	2.4E-5
Boron steel	200	0.30	--	1.2E-5

boron steel rivet and the aluminium alloy AA5754 sheets undergo large plastic deformations and thus were modelled as elastic-plastic bodies, the mechanical properties of the boron steel rivet and the AA5754 sheets are listed in Table 1. The plastic stress-strain curves considering the temperature effect of the AA5754 are used to model the sheet deformations as shown in Fig. 4a. The temperature change during the joining process (20~250 °C) has very limited influence on the rivet properties [25], and thus, only the plastic stress-strain curve at 20 °C of the boron steel is used to model the rivet deformation as shown in Fig. 4b.

To make a balance between the simulation efficiency and accuracy, the mesh size of the rivet and the top sheet was set to 0.10 mm, but the mesh size of the bottom sheet was set to 0.12 mm. Quad element with four gauss points was used for all the deformation parts. Automatic element re-meshing was applied on the two sheets to deal with the large material deformation during the riveting process. A geometric criterion was employed to model the top sheet separation, and the critical thickness was set to 0.04 mm. The Coulomb friction model was used to describe the frictions between contact parts. The friction coefficients listed in Table 2 are identified using the inverse method. More details about the FEA simulation model can be found in the authors' previous study [26].

2.1.2 Model validation

The capability and accuracy of the developed FEA model were verified by comparing the simulated joint quality results with the experimental SPR test results. As listed in Table 3, twenty-five groups of aluminium alloy AA5754 joints with different sheets, rivet and die combinations are generated using the Tucker servo SPR system shown in Fig. 5. Three rivets with different lengths (L_1) (i.e. 5.0 mm, 6.0 mm and 6.5 mm) and six dies with different diameters (D_1) and depths (H_1) were used in the experiments. The cross-sectional profiles of the semi-tubular rivet and the pip die are illustrated in Fig. 6. The nominal rivet shank diameter and rivet hardness are Ø5.3 mm and 280 ± 30HV10, respectively. The die pip height (H_2) is fixed at 0.0 mm in all dies. The specimen size is 40 mm × 40 mm as shown in Fig. 7, and at least three repetitions for each group are made. All the specimens were sectioned through the joint central axis and polished. Then, the joint cross-sectional profile is inspected using an optical microscope, and the three quality indicators (i.e. the rivet head height, the interlock and the T_{min} shown in Fig. 2) are measured.

The twenty-five SPR joints were also simulated with the developed FEA model. The magnitude of the rivet head height is highly associated with the final values of the interlock and T_{min} [6]. To properly evaluate the prediction accuracy of the FEA model, the measured rivet head height from the experimental test (listed in Table 3) was implemented as the termination criterion of the corresponding SPR simulation. The simulated joint cross-sectional profile, interlock and T_{min} were also recorded for each joint.

The joint cross-sectional profiles from the experimental tests and the FEA model are given in Fig. 8. For easier comparisons, half of the simulated joint profiles were superimposed on the tested ones. It can be identified that there

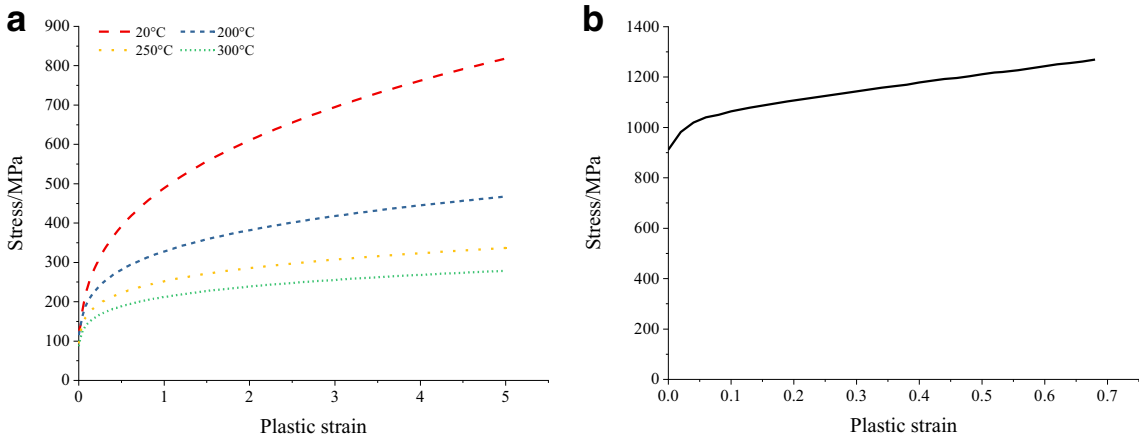

Fig. 4 Plastic stress-strain curves for (**a**) the AA5754 (strain rate = 1 s^{-1}) [25] and (**b**) the boron steel rivet (20 °C, strain rate = 0.01 s^{-1}) [26]

Table 2 Friction coefficients between the different parts in FEA simulation model [26]

Contact pairs	Punch-rivet	Blank holder-sheets	Rivet-sheets	Top sheet-bottom sheet	Bottom sheet-die	Others
Friction coefficients	0.10	0.10	0.10	0.10	0.22	0.10

are no gross differences between the simulated and experimental joint profiles. The local material deformation of the bottom sheet (e.g. zone 1 and zone 2) and the gaps between the rivet and top sheet (e.g. zone 3 and zone 4) were successfully captured by the FEA model. To quantitatively evaluate the prediction accuracy of the FEA model, the bottom sheet thickness at the joint centre (T_c), the horizontal bottom sheet thickness beside the rivet tip (T_h) and the deformed rivet shank radius (R_f) are measured on the tested and simulated profiles shown in Fig. 8. Comparisons between the simulated and the tested three indicators are given in Fig. 9. The calculated mean absolute errors (MAE) between the simulation and experimental results for the T_c, R_f and T_h were 0.060 mm, 0.073 mm and 0.066 mm, respectively. The calculated mean absolute percentage errors (MAPE) for the T_c, R_f and T_h were 13.59%, 1.94% and 10.64%, respectively. Therefore, it can be concluded that the developed FEA model has the capability to predict the joint cross-sectional profile. The average values of the interlock and the T_{min} obtained from the simulated and the tested joints are listed in Table 3 and illustrated in Fig. 10. The calculated MAE between the simulation and experimental results for the interlock and the T_{min} were 0.037 mm and 0.045 mm, respectively, and the corresponding MAPE were 6.75% and 9.53%. The Pearson's correlation coefficient (r) between

Table 3 Joint configurations and the results for validation of the FEA model

Joint configurations					Experimental and simulation results					
Joint no.	Stack/mm (AA5754)	Rivet length L_1/mm	Die		Rivet head height/mm		Interlock/mm		T_{min}/mm	
			Diameter D_1/mm	Depth H_1/mm	Tested (Mean)	Simulated	Tested (Mean)	Simulated	Tested (Mean)	Simulated
E1	1.0 + 1.8	5.0	8.0	2.0	− 0.09	− 0.1	0.59	0.58	0.40	0.35
E2	1.2 + 1.0	5.0	8.0	2.0	− 0.10	− 0.1	0.48	0.50	0.12	0.13
E3	1.2 + 1.5	5.0	8.0	2.0	− 0.07	− 0.1	0.51	0.52	0.33	0.31
E4	1.2 + 1.8	5.0	8.0	2.0	− 0.10	− 0.1	0.53	0.51	0.53	0.48
E5	1.2 + 2.0	5.0	8.0	2.0	− 0.09	− 0.1	0.52	0.55	0.72	0.72
E6	1.2 + 1.8	6.0	8.0	2.0	− 0.14	− 0.1	0.86	0.73	0.24	0.26
E7	1.5 + 1.5	5.0	9.0	1.6	0.00	0.0	0.42	0.38	0.53	0.51
E8	1.2 + 1.8	5.0	9.0	1.6	− 0.11	− 0.1	0.59	0.60	0.47	0.46
E9	1.2 + 2.0	6.0	9.0	1.6	0.05	0.0	0.94	0.85	0.38	0.30
E10	1.8 + 2.0	6.0	9.0	1.6	0.08	− 0.1	0.70	0.67	0.67	0.74
E11	2.5 + 2.0	6.0	9.0	1.6	0.10	− 0.1	0.31	0.35	0.93	0.90
E12	1.2 + 1.2	5.0	10.0	1.8	− 0.08	− 0.1	0.36	0.32	0.24	0.28
E13	1.2 + 1.8	5.0	10.0	1.8	− 0.07	− 0.1	0.48	0.47	0.48	0.50
E14	1.8 + 1.2	5.0	10.0	1.8	− 0.07	− 0.1	0.13	0.13	0.63	0.63
E15	1.8 + 1.8	5.0	10.0	1.8	− 0.11	− 0.1	0.30	0.25	1.26	1.04
E16	1.0 + 1.8	5.0	10.0	2.0	− 0.04	− 0.1	0.49	0.51	0.44	0.37
E17	1.2 + 1.5	5.0	10.0	2.0	− 0.03	− 0.1	0.34	0.36	0.40	0.36
E18	1.2 + 1.8	5.0	10.0	2.0	− 0.04	− 0.1	0.47	0.44	0.62	0.53
E19	1.2 + 2.0	5.0	10.0	2.0	− 0.06	− 0.1	0.49	0.46	0.67	0.69
E20	1.5 + 1.8	5.0	10.0	2.0	− 0.05	− 0.1	0.33	0.31	0.85	0.77
E21	2.0 + 1.8	5.0	10.0	2.0	− 0.03	− 0.1	0.18	0.19	1.24	1.25
E22	1.2 + 1.8	6.0	10.0	2.0	− 0.13	− 0.1	0.90	0.84	0.28	0.24
E23	1.2 + 1.8	6.5	10.0	2.0	− 0.09	− 0.1	1.20	1.05	0.22	0.14
E24	1.2 + 1.8	5.0	11.0	1.8	− 0.07	− 0.1	0.36	0.37	0.56	0.52
E25	1.2 + 1.8	5.0	11.0	2.0	− 0.02	− 0.1	0.40	0.35	0.60	0.58

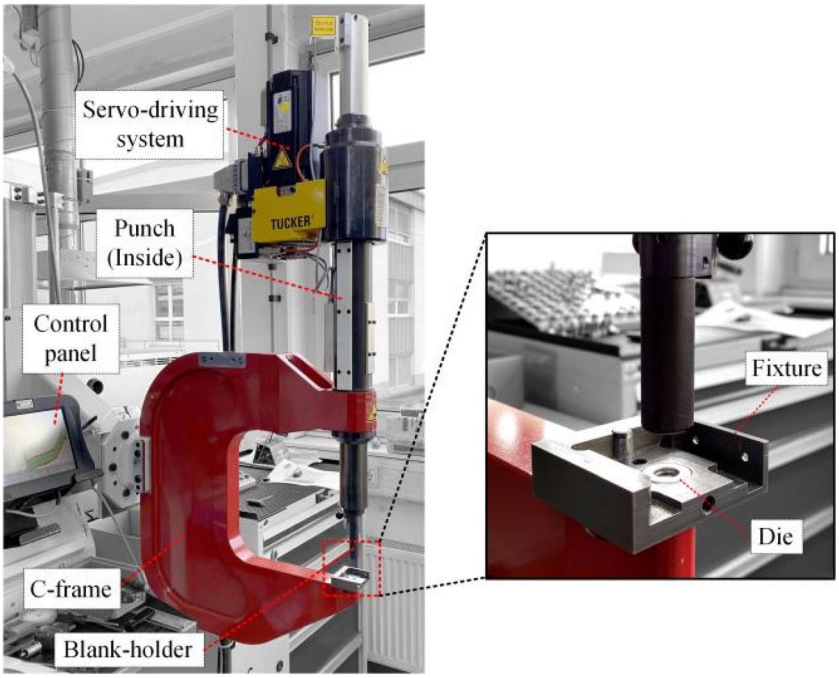

Fig. 5 Structure of the Tucker SPR system

the experimental and simulation results was also calculated. The calculated r for the interlock and the T_{min} was 0.988 and 0.981, respectively. Therefore, the interlock and T_{min} values were accurately predicted by the FEA simulation model.

From the analysis and comparisons above, it is reasonable to confirm that the developed FEA model is capable of predicting the quality and material deformation of SPR joints (boron steel rivet + AA5754 sheets) with varying rivet and die profiles.

2.1.3 Orthogonal test

When collecting the joint quality data for further mathematical model development, the orthogonal design method was adopted to minimize the total number of SPR simulations required. The rivet length (L_1), die diameter (D_1) and depth (H_1) are the three independent variables, and each independent variable has three levels as listed in Table 4. The hardness of the Ø5.3 mm boron steel rivets is 280 ± 30HV10. The die geometries are modified based on the reference die in Fig. 11 (D_1 = 9.0 mm, H_1 = 1.6 mm, H_2 = 0.0 mm). Moreover, to investigate the interaction effects of the L_1, D_1 and H_1 on the joint quality, the interaction terms ($L_1 \times D_1$, $L_1 \times H_1$ and $D_1 \times H_1$) between these independent variables were also considered in the orthogonal test. According to the number of independent variables, interaction terms and levels, the L_{27} (3^{13}) orthogonal table with 13 columns and 27 rows is selected (Table 5). Four null columns were left and treated as error terms.

All the 27 SPR joints with different configurations in Table 5 are made using the developed FEA simulation model. For consistency, all the simulations were terminated when the rivet head height reached to 0.0 mm. By observing all the 27 simulated joint cross-sectional profiles, it was found that the T_{min} appeared around the rivet tip in most of the joints. Therefore, to keep the data uniformity and make it easier for the mathematical prediction model development, the minimum bottom sheet thickness around the rivet tip in all the 27 joints was measured as the T_{min} in this study. Table 5 shows the simulated values of interlock and T_{min} for the 27 SPR joints.

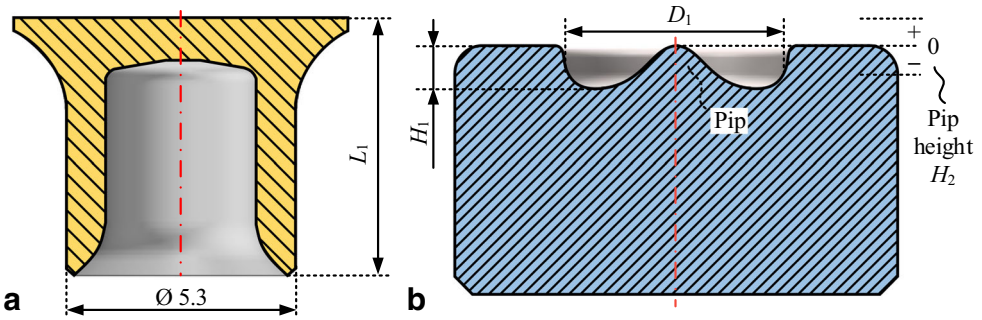

Fig. 6 Schematics of (**a**) the semi-tubular rivet and (**b**) the pip die

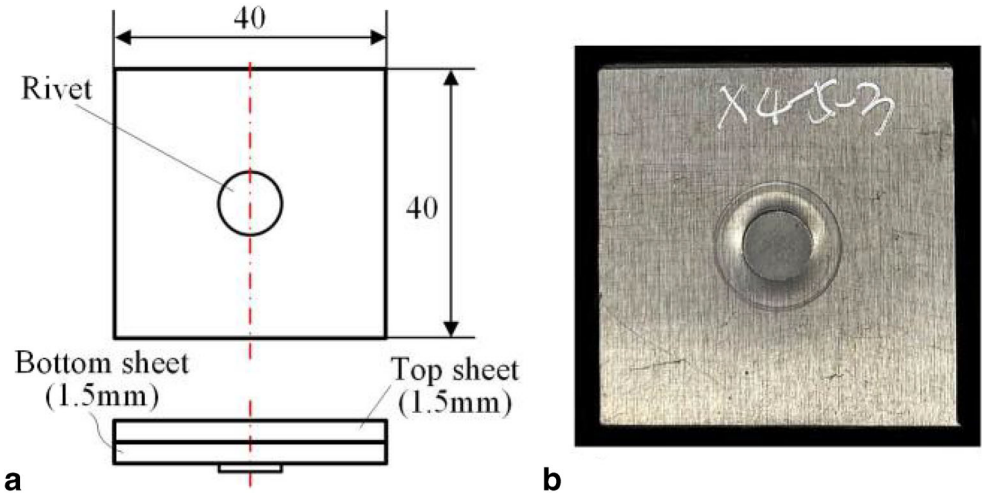

Fig. 7 Dimensions of the SPR specimen

3 Mathematic prediction models for the interlock and the T_{min}

3.1 Analysis of variance (ANOVA)

The analysis of variance (ANOVA) was performed using the orthogonal test results to evaluate the significances of the three independent variables (L_1, D_1 and H_1) and their interaction terms ($L_1 \times D_1$, $L_1 \times H_1$ and $D_1 \times H_1$) on the interlock and the T_{min} with software Minitab 19. Tables 6 and 7 list the results of the ANOVA for the interlock and the T_{min}, respectively. In general, the smaller the p value is, the more significant the variable is. The influence of a variable on the response is considered as significant if the corresponding p value is smaller than 0.05 or 0.10, depending on the selected significant level (0.05 or 0.10). It was apparent that all the three independent variables and their interaction terms had significant influences on the interlock as the p values were

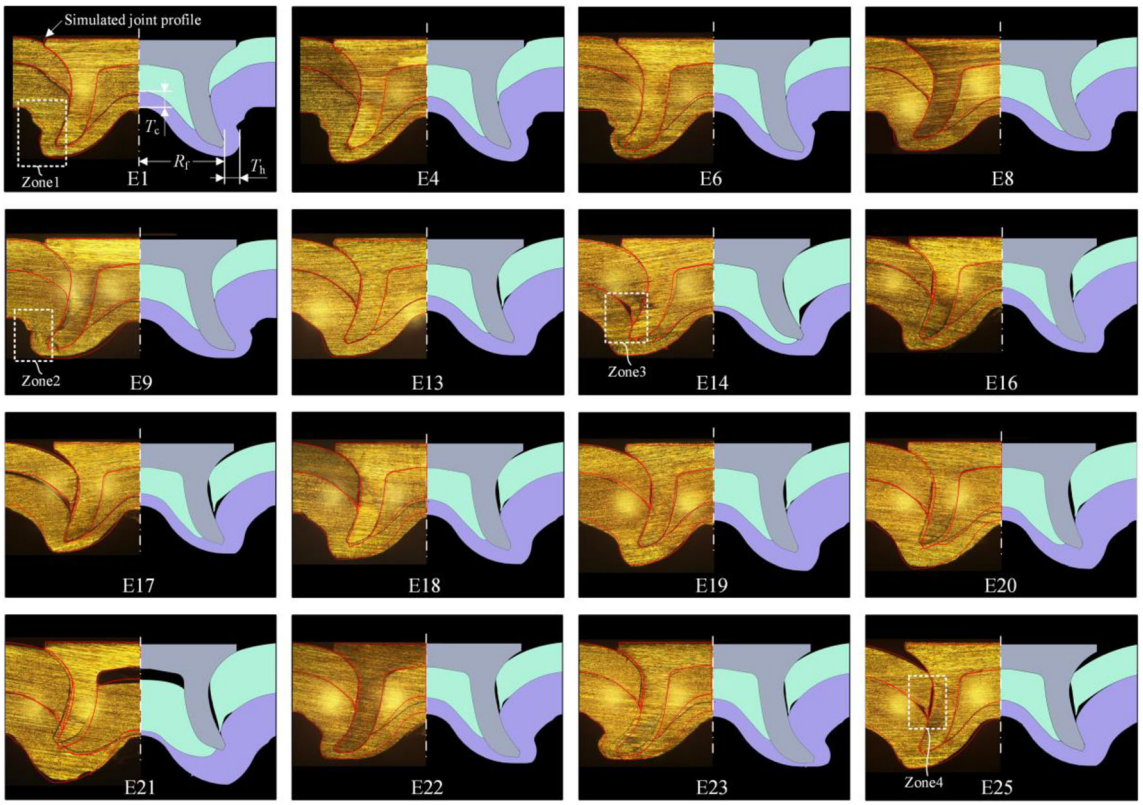

Fig. 8 Comparisons of the joint cross-sectional profiles from the experimental tests and FEA simulations

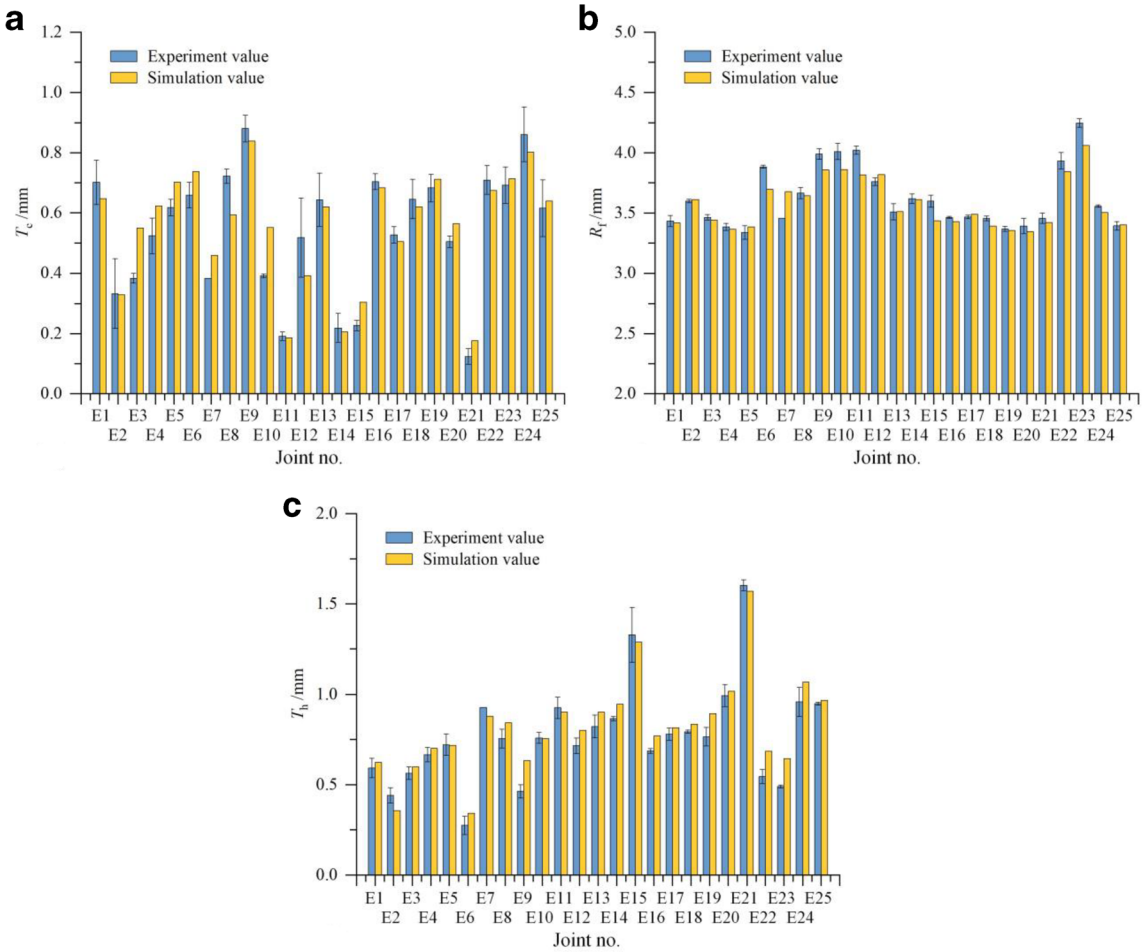

Fig. 9 Comparisons of (a) the T_c, (b) the R_f and (c) the T_h from experimental tests and FEA simulations

less than 0.05. However, under the studied joint configurations, the rivet length (L_1) showed a significant influence on the T_{min}, while the other two independent variables (D_1 and H_1) and the three interaction terms ($L_1 \times D_1$, $L_1 \times H_1$ and $D_1 \times H_1$) did not show remarkable effect on the T_{min}.

3.2 Development of the regression models

Multiple regression analysis was carried out using the software Minitab 19 to develop the prediction models for the interlock and T_{min}. According to the results of ANOVA, the

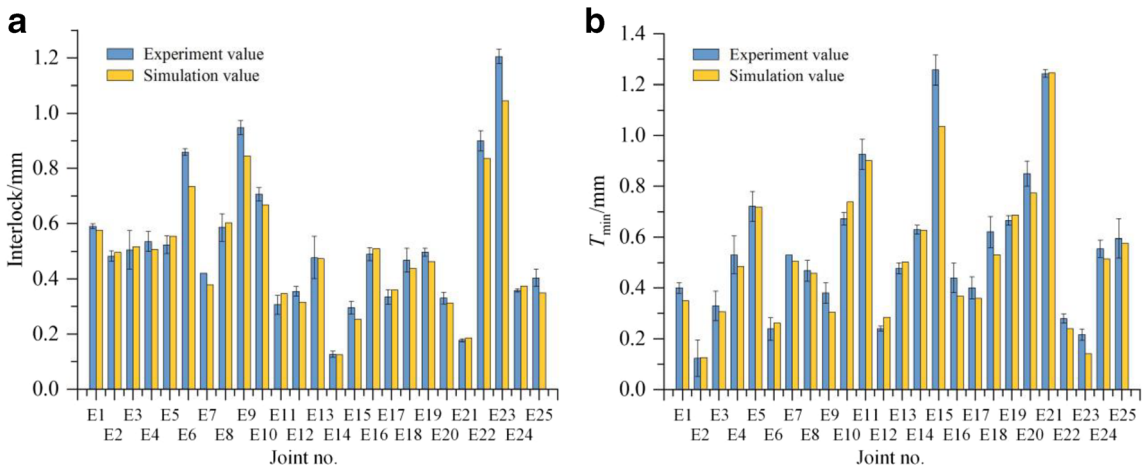

Fig. 10 Comparisons of (a) the interlock and (b) the T_{min} from experimental tests and FEA simulations

Table 4 Independent variables and levels of the orthogonal test

Level	Rivet length L_1/mm	Die diameter D_1/mm	Die depth H_1/mm
1	5	8.0	1.6
2	6	9.0	1.8
3	6.5	10.0	2.0

three independent variables and the three interaction terms were significant for the interlock. So all of them were included in the multiple regression model of interlock in Eq. (1). As for the $T_{\min}$, although only the rivet length was a statistically significant variable under the studied joint configurations, the influences of other variables on the $T_{\min}$ were also considered in this study. Therefore, all of them are also involved in the regression model of $T_{\min}$ in Eq. (2).

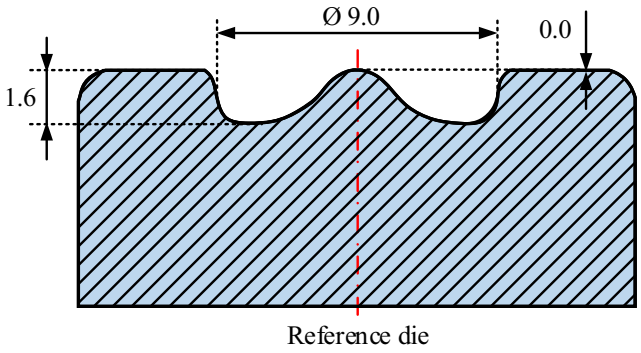

Fig. 11 Dimonsions of the reference pip die

$$Interlock = \alpha_0 + \alpha_1 L_1 + \alpha_2 D_1 + \alpha_3 H_1 + \alpha_4 L_1 \times D_1 + \alpha_5 L_1 \times H_1 + \alpha_6 D_1 \times H_1 \quad (1)$$

Table 5 L_{27} (3^{13}) orthogonal test design and simulation results

Joint No.	Variables and levels													Simulation results	
	L_1	D_1	$(L_1 \times D_1)$ 1	$(L_1 \times D_1)$ 2	H_1	$(L_1 \times H_1)$ 1	$(L_1 \times H_1)$ 2	$(D_1 \times H_1)$ 1	Null	Null	$(D_1 \times H_1)$ 2	Null	Null	Interlock /mm	$T_{\min}$ /mm
S-1	1	1	1	1	1	1	1	1	1	1	1	1	1	0.37	0.56
S-2	1	1	1	1	2	2	2	2	2	2	2	2	2	0.39	0.55
S-3	1	1	1	1	3	3	3	3	3	3	3	3	3	0.35	0.52
S-4	1	2	2	2	1	1	1	2	2	2	3	3	3	0.38	0.51
S-5	1	2	2	2	2	2	2	3	3	3	1	1	1	0.33	0.50
S-6	1	2	2	2	3	3	3	1	1	1	2	2	2	0.27	0.52
S-7	1	3	3	3	1	1	1	3	3	3	2	2	2	0.28	0.56
S-8	1	3	3	3	2	2	2	1	1	1	3	3	3	0.24	0.57
S-9	1	3	3	3	3	3	3	2	2	2	1	1	1	0.20	0.59
S-10	2	1	2	3	1	2	3	1	2	3	1	2	3	0.57	0.26
S-11	2	1	2	3	2	3	1	2	3	1	2	3	1	0.60	0.32
S-12	2	1	2	3	3	1	2	3	1	2	3	1	2	0.61	0.34
S-13	2	2	3	1	1	2	3	2	3	1	3	1	2	0.74	0.26
S-14	2	2	3	1	2	3	1	3	1	2	1	2	3	0.71	0.27
S-15	2	2	3	1	3	1	2	1	2	3	2	3	1	0.70	0.25
S-16	2	3	1	2	1	2	3	3	1	2	2	3	1	0.59	0.27
S-17	2	3	1	2	2	3	1	1	2	3	3	1	2	0.55	0.28
S-18	2	3	1	2	3	1	2	2	3	1	1	2	3	0.52	0.25
S-19	3	1	3	2	1	3	2	1	3	2	1	3	2	0.62	0.16
S-20	3	1	3	2	2	1	3	2	1	3	2	1	3	0.66	0.20
S-21	3	1	3	2	3	2	1	3	2	1	3	2	1	0.69	0.24
S-22	3	2	1	3	1	3	2	2	1	3	3	2	1	0.89	0.23
S-23	3	2	1	3	2	1	3	3	2	1	1	3	2	0.88	0.23
S-24	3	2	1	3	3	2	1	1	3	2	2	1	3	0.86	0.20
S-25	3	3	2	1	1	3	2	3	2	1	2	1	3	0.75	0.26
S-26	3	3	2	1	2	1	3	1	3	2	3	2	1	0.75	0.19
S-27	3	3	2	1	3	2	1	2	1	3	1	3	2	0.72	0.18

Table 6 Results of ANOVA for the interlock

Source	DF	Adj SS	Adj MS	*F* value	*p* value
L_1	2	0.93608	0.468041	4322.59	0.000
D_1	2	0.08224	0.041120	379.77	0.000
$L_1 \times D_1$	4	0.06324	0.01581	146.00	0.000
H_1	2	0.00424	0.002121	19.59	0.001
$L_1 \times H_1$	4	0.00465	0.001163	10.74	0.003
$D_1 \times H_1$	4	0.00937	0.00234	21.64	0.000
Error	8	0.00087	0.000108	--	--
Total	26	1.10069	--	--	--

$$T_{\min} = \beta_0 + \beta_1 L_1 + \beta_2 D_1 + \beta_3 H_1 + \beta_4 L_1 \cdot D_1 + \beta_5 L_1 \cdot H_1 + \beta_6 D_1 \cdot H_1 \quad (2)$$

The unknown coefficients in the regression models (the α_0 to α_6 and the β_0 to β_6) were identified with the orthogonal test results by the software Minitab 19. The final regression models of interlock and $T_{\min}$ are shown in Eqs. (3). and (4).

$$Interlock = 2.030 - 0.543 L_1 - 0.196 D_1 + 0.280 H_1 + 0.069 L_1 \cdot D_1 + 0.125 L_1 \cdot H_1 - 0.120 D_1 \cdot H_1 \quad (3)$$

$$T_{\min} = -0.360 - 0.093 L_1 + 0.206 D_1 + 0.793 H_1 - 0.012 L_1 \cdot D_1 - 0.016 L_1 \cdot H_1 - 0.076 D_1 \cdot H_1 \quad (4)$$

3.3 Evaluation of the regression models

The fitting accuracy of the regression model was evaluated statistically by five indicators. The coefficient of determination (R^2) describes how close the predicted and the actual values lie, and the R^2 close to 1 indicates the good fitting achieved using this regression model. The adjusted R^2 (R^2_{adj}), which is effective at eliminating the influence of the independent variables' numbers, was also used to evaluate the accuracy of the regression models. Meanwhile, the prediction R^2 (R^2_{pred}), the mean absolute error (MAE) and the standard error (S) were also employed to further assess the model accuracy. The evaluation results for the regression models of interlock and $T_{\min}$ are listed in Table 8. Both of the R^2 and R^2_{adj} for the interlock were over 0.860, and the value of the R^2_{pred} was up to 0.828. The corresponding MAE and S values for the interlock were 0.055 mm and 0.076 mm. For the $T_{\min}$, the R^2, R^2_{adj} and R^2_{pred} were as high as 0.949, 0.934 and 0.885, respectively. The corresponding MAE and S values were 0.029 mm and 0.039 mm. Therefore, the developed regression models are accurate enough to predict the interlock and the $T_{\min}$. In other words, it is proved that the developed multiple regression models could be used to replace this FEA simulation model for the SPR joint quality prediction under the studied joint configurations.

Table 7 Results of ANOVA for the $T_{\min}$

Source	DF	Adj SS	Adj MS	*F* value	*p* value
L_1	2	0.561094	0.280547	266.93	0.000
D_1	2	0.002480	0.001240	1.18	0.356
$L_1 \times D_1$	4	0.00833	0.00208	1.98	0.191
H_1	2	0.000168	0.000084	0.08	0.924
$L_1 \times H_1$	4	0.00071	0.00018	0.17	0.948
$D_1 \times H_1$	4	0.00324	0.00081	0.77	0.574
Error	8	0.008408	0.001051	--	--
Total	26	0.584434	--	--	--

3.4 Validation of the regression models

To verify the performance of the developed regression models in real applications, seven groups of SPR joints with different rivets and dies, as shown in Table 9, were made using laboratory experimental tests. Three repetitions for each group were performed. The average values of the interlock and the $T_{\min}$ from the experimental SPR tests and the predicted values from the regression models are recorded in Table 9 and compared graphically in Fig. 12. The calculated MAE between the predicted and experimental results for the interlock and the $T_{\min}$ were 0.047 mm and 0.053 mm, respectively, and the corresponding MAPE were 10.4% and 12.3%. The calculated Pearson's correlation coefficient (r) for the interlock and $T_{\min}$ were 0.987 and 0.964, respectively. Thus, the predicted interlock and $T_{\min}$ matched well with the experimental results. This also indicated the high prediction accuracy of the developed regression models for the interlock and the $T_{\min}$.

According to the statistic evaluation and experimental verification results, it is reasonable to conclude that the developed multiple regression models are effective for quality prediction of the studied SPR joints. Meanwhile, the model development method used in this study is also proved to be valid.

Table 8 Evaluation results of the regression models for the interlock and $T_{\min}$

	R^2	R^2_{adj}	R^2_{pred}	MAE/ mm	S/ mm
Interlock	0.896	0.865	0.828	0.055	0.076
$T_{\min}$	0.949	0.934	0.885	0.029	0.039

Table 9 Joint configurations and the results for the validation of the regression models

Joint configurations					Experimental and predicted results					
Joint no.	Stack/mm (AA5754)	Rivet length L_1/mm	Die		Rivet head height/mm		Interlock/mm		T_{min}/mm	
			Diameter D_1/mm	Depth H_1/mm	Tested (Mean)	Predicted	Tested (Mean)	Predicted	Tested (Mean)	Predicted
E26	1.5 + 1.5	5.0	8.0	2.0	− 0.04	0	0.35	0.40	0.57	0.55
E27		5.0	9.0	1.6	0.02	0	0.42	0.38	0.53	0.54
E28		5.0	10.0	1.8	− 0.07	0	0.33	0.27	0.59	0.55
E29		5.0	10.0	2.0	− 0.05	0	0.25	0.22	0.66	0.54
E30		6.0	9.0	1.6	0.02	0	0.69	0.66	0.36	0.31
E31		6.0	10.0	1.8	− 0.05	0	0.69	0.65	0.38	0.31
E32		6.5	10.0	1.8	− 0.06	0	0.91	0.83	0.25	0.19

4 Interaction analysis between the rivet and die parameters on the interlock and the T_{min}

Unlike the experimental SPR test or the FEA simulation model, the interaction effects between different joining parameters on the joint quality can be easily inspected by observing the contour graphs drawn from the developed regression models. In this section, the interaction effects between the rivet and die parameters (L_1, D_1 and H_1) on the interlock and the T_{min} were systematically analysed. Some simulated joint cross-sectional profiles are also presented to further verify the contour graphs and to explain the changing trends of the interlock and the T_{min}. All the discussions were carried out on the basis of a uniform rivet head height (0.0 mm). To avoid repetition, not all representative contour graphs and interaction effects were presented and discussed in detail.

4.1 Interaction effects between the L_1 and D_1

When the die depth (H_1) was fixed at 1.8 mm, the contour graphs of the interlock and the T_{min} with varying rivet length (L_1) and die diameter (D_1) are plotted in Fig. 13. Apparent interaction effects between the rivet length and die diameter on the interlock were indicated by the non-parallel lines shown in Fig. 13(a). With the die diameter increased from 8.0 to 10.0 mm, the interlock demonstrated a decreasing trend when the rivet length was smaller than 6.0 mm, but an increasing tendency when the rivet length was greater than 6.0 mm. With the rivet length increased from 5.0 to 6.5 mm, a higher increasing rate (a larger gradient density) of the interlock was observed when the die had a larger diameter. In contrast, very weak interaction effects on the T_{min} were found because of the almost parallel contour lines in Fig. 13(b). When the die diameter increased from 8.0 to 10.0 mm, the T_{min} kept almost constant with different rivet lengths. While when the rivet length increased from 5.0 to 6.5 mm, the T_{min} rapidly decreased at almost the same rate with different die diameters. The rivet length almost dominated the magnitude of the T_{min}, which is in agreement with the ANOVA results in Table 7.

To assist the contour graph analysis, the simulated joint cross-sectional profiles at the points a~i in Fig. 13 are presented in Fig. 14. In both figures, the interlock showed an increasing trend as the rivet length increased, but irregular changes

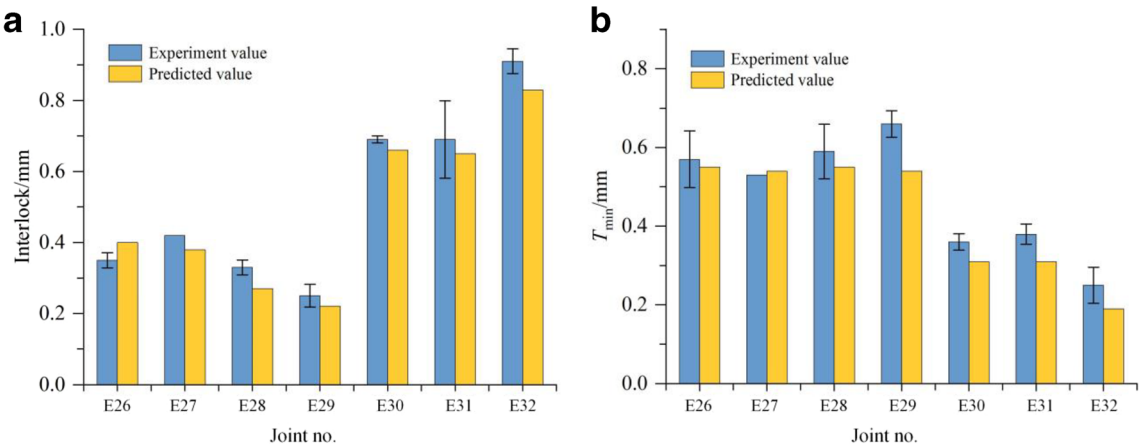

Fig. 12 Comparisons between the experimental values and the predicted values using the regression models: (a) the interlock and (b) the T_{min}

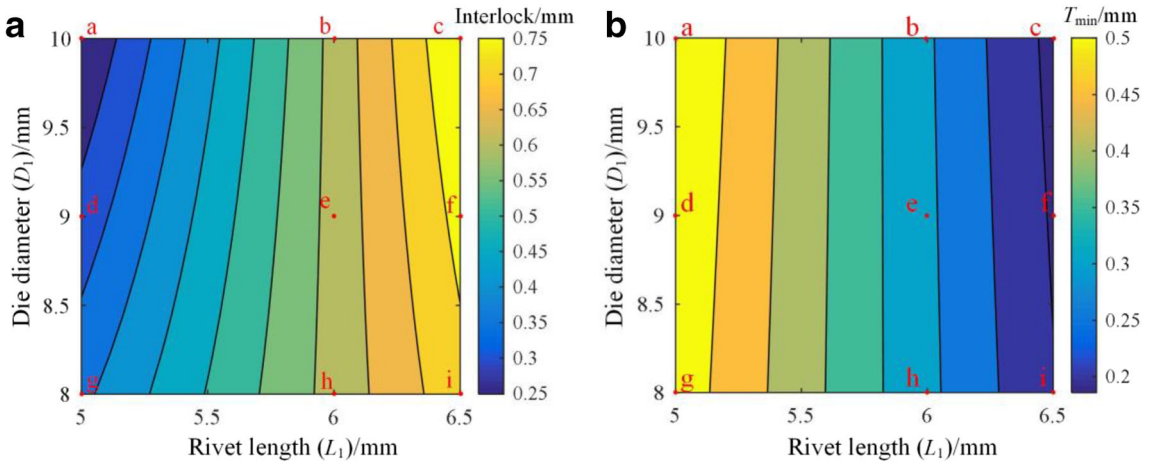

Fig. 13 Contour graphs of (a) the interlock and (b) the T_{min} with different rivet lengths and die diameters (die depth = 1.8 mm)

when the die diameter varied. In contrast, the T_{min} decreased as the rivet length increased but remained almost constant as the die diameter increased. A good agreement between the predicted results from the developed regression models and the FEA simulation model was found, except for the interlock values in Fig. 14e and f underestimated by the regression model. This might be attributed to the inherent limitation of the adopted regression model, which could only describe a monotonous growth or decline trend.

Such interaction effects between the rivet and die parameters on the interlock are attributed directly to the deformation behaviour of the rivet and the sheets. As key components in the SPR process, the rivet is used to pierce through the top sheet and flare into the bottom sheet. The specially designed die is used to guide the rivet flaring and the sheet deforming into its cavity. To achieve a sound SPR joint with a flush head height (approx. 0.0 mm), the rivet volume (V_r) should be equal to the die cavity volume (V_d) or slightly larger if considering

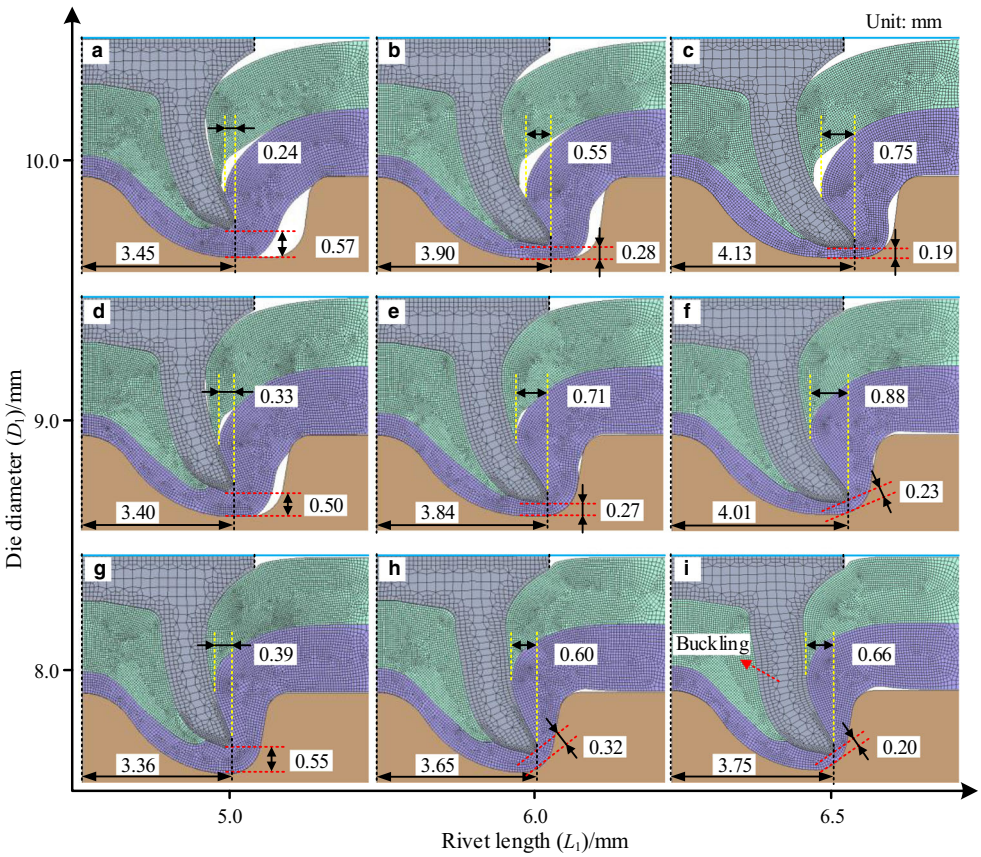

Fig. 14 Simulated joint cross-sectional profiles with different rivet lengths and die diameters (H_1 = 1.8 mm) (**a**) L_1 = 5.0 mm, D_1 = 10.0 mm (**b**) L_1 = 6.0 mm, D_1 = 10.0 mm (**c**) L_1 = 6.5 mm, D_1 = 10.0 mm (**d**) L_1 = 5.0 mm, D_1 = 9.0 mm (**e**) L_1 = 6.0mm, D_1 = 9.0 mm (**f**) L_1 = 6.5 mm, D_1 = 9.0 mm (**g**) L_1 = 5.0 mm, D_1 = 8.0 mm (**h**) L_1 = 6.0 mm, D_1 = 8.0 mm and (**i**) L_1 = 6.5 mm, D_1 = 8.0 mm

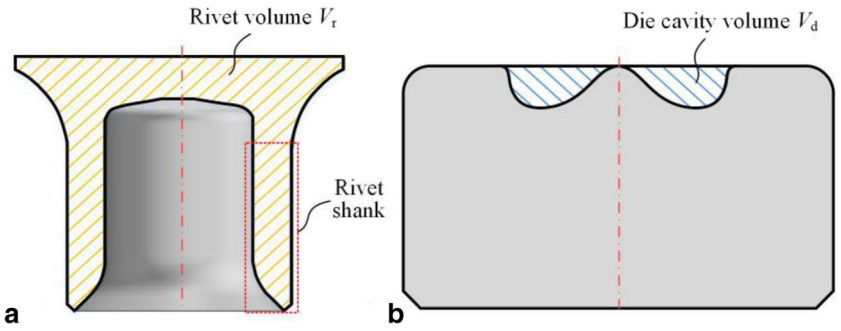

Fig. 15 Schematic of (a) the rivet volume V_r and (b) the die cavity volume V_d

the rivet and sheet material compressions, as shown in Fig. 15. Table 10 lists the volumes of the rivets and the dies used in this study. In practice, if the V_d was much smaller than the V_r, as shown in Fig. 16(a), the die cavity could not accommodate all the material pressed into it. Once the die cavity was fully filled, the die would provide a high resistance force to prevent further downward movement of the rivet. This would lead to buckling of the rivet shank and impose negative effects on the interlock formation. In contrast, if the V_d became much larger than the V_r by increasing the die diameter (D_1) as shown in the Fig. 16b, there will be always a void space underneath the bottom sheet. So, the bottom sheet became easier to be deformed into the die cavity and imposed less resistance force on the outer surface of the rivet shank (F_{out}). While the resistance force applied on the inner surface of the rivet shank (F_{in}) kept almost unchanged considering the similar filling conditions of the rivet cavity. As a result, the rivet shank flared a larger distance, but was not effectively inserted into the bottom sheet to form the interlock. Therefore, the maximum interlock value would be always achieved when the V_d was close to the V_r, in which the rivet shank could be inserted effectively into the bottom sheet to form the interlock without buckling.

When the die diameter increased from 8.0 to 10.0 mm, due to the different initial die-to-rivet volume ratios ($R = V_d/V_r$), the interlock demonstrated different changing trends at 5.0 mm, 6.0 mm and 6.5 mm rivet lengths. For the 5.0-mm long rivets, the values of the R in Fig. 14g, d and a were 0.88, 1.14 and 1.44, respectively, which resulted in a rapid decrease of the interlock from 0.39 to 0.24 mm. While for the 6.0- and 6.5-mm rivets, severe rivet shank buckling is observed in Fig. 14h and i due to the small values of the R (0.77 and 0.73). With the increment of the die diameter, the reduction of the rivet shank buckling imposed a positive effect on the interlock formation in Fig. 14e and f, but then, the interlock decreased when the R became much larger (i.e. 1.26 in Fig. 14b and 1.19 in Fig. 14c). Thus, with the 6.0 and 6.5 mm rivets, the interlock first increased but then decreased as the die diameter increased.

When the rivet length increased from 5.0 to 6.5 mm, the interlock had a smaller increasing speed with the 8.0 mm die diameter shown in Fig. 14. This is because the rivet shank underwent more and more severe buckling with the reduction of the R value.

4.2 Interaction effects between the L_1 and H_1

Figure 17 shows the contour graphs of the interlock and the T_{min} with different rivet lengths (L_1) and die depths (H_1) when the die diameter (D_1) was fixed at 9.0 mm. As shown in Fig. 17(a), significant interaction effects indicated by the non-parallel lines are also found on the interlock. When the die depth increased from 1.6 to 2.0 mm, the interlock showed a decreasing trend, and its reducing speed slowly decreased as the rivet length increasing from 5.0 to 6.0 mm. Once the rivet length became greater than 6.0 mm, the interlock remained

Table 10 Rivet volumes and die cavity volumes

Rivet		Die		
Length L_1/mm	Volume V_r/mm^3	Diameter D_1/mm	Depth H_1/mm	Volume V_d/mm^3
5.0	90.0	8.0	1.6	70.07
			1.8	79.54
			2.0	89.07
6.0	102.3	9.0	1.6	91.58
			1.8	103.02
			2.0	111.03
6.5	108.6	10.0	1.6	116.21
			1.8	129.26
			2.0	142.84

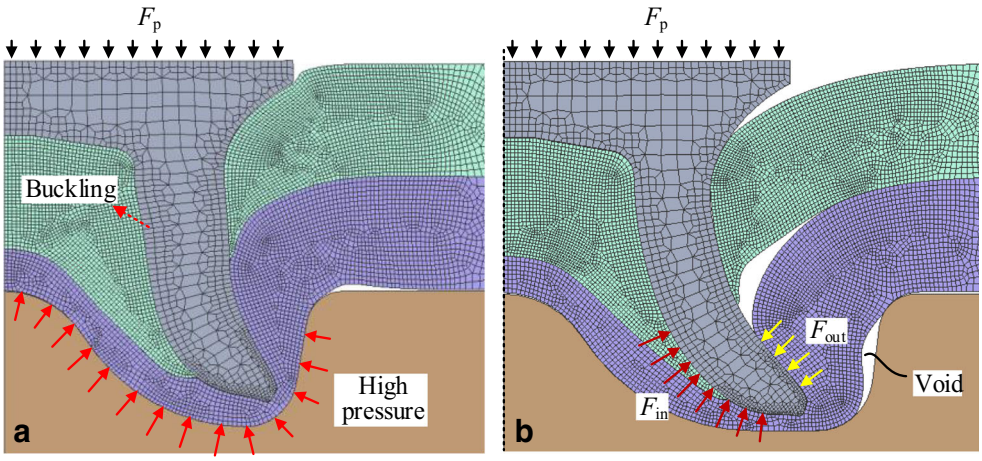

Fig. 16 Joint cross-sectional profiles with (a) $V_d < V_r$ and (b) $V_d > V_r$ during the SPR processes

almost constant with the increment of the die depth. In contrast, the parallel lines shown in Fig. 17(b) indicate the very weak interaction effects on the T_{min}. The rivet length showed a dominant influence on the value of the T_{min}, while the die depth demonstrated little effect on the T_{min} under the studied joint configurations. The simulated joint cross-sectional profiles at points a~i in Fig. 17 are presented in Fig. 18. It can be seen from these two figures that the predicted joint quality by the developed regression models matched well with that from the FEA simulation model. For a given die depth, the interlock increased but T_{min} decreased as the rivet length increased. For a given rivet length, the interlock decreased, but the T_{min} remained almost unchanged as the die depth increased.

The increment of die depth could also increase the V_d and result in a larger die-to-rivet volume ratio (R). While different from the die diameter, a larger die depth could lead to an easier downward movement of the bottom sheet. As a result, the rivet shank flared less and a smaller interlock was formed. Such effect was more significant for the 5.0 mm long rivets than the 6.0 mm and 6.5 mm rivets: the interlock showed a larger decrease with the 5.0 mm long rivets but reduced a smaller value with the 6.0 mm and 6.5 mm rivets because of the reduction of the rivet shank buckling degrees in Fig. 18e and f.

4.3 Interaction effects between the D_1 and H_1

When the rivet length (L_1) was fixed at 5.0 mm, the contour graphs of the interlock and the T_{min} with different die diameters (D_1) and depths (H_1) are shown in Fig. 19. Significant interaction effects were indicated by the non-parallel lines on the interlock, as shown in Fig. 19(a). When the die depth increased from 1.6 to 2.0 mm, the interlock decreased at a slower speed with a small diameter die (e.g. D_1 = 8.0 mm) than with a larger one (e.g. D_1 = 10.0 mm). Similarly, when the die diameter increased from 8.0 to 10.0 mm, the interlock also showed a smaller decreasing speed with a small depth die (e.g. H_1 = 1.6 mm) than with a larger one (e.g. H_1 = 2.0 mm). However, considering the relatively small changing range (from 0.51 to 0.555 mm) of the T_{min} in Fig. 19(b) and the prediction accuracy of the regression model (MAE = 0.029 mm), the interaction effects on the T_{min} were not confident to be evaluated and therefore not discussed in detail.

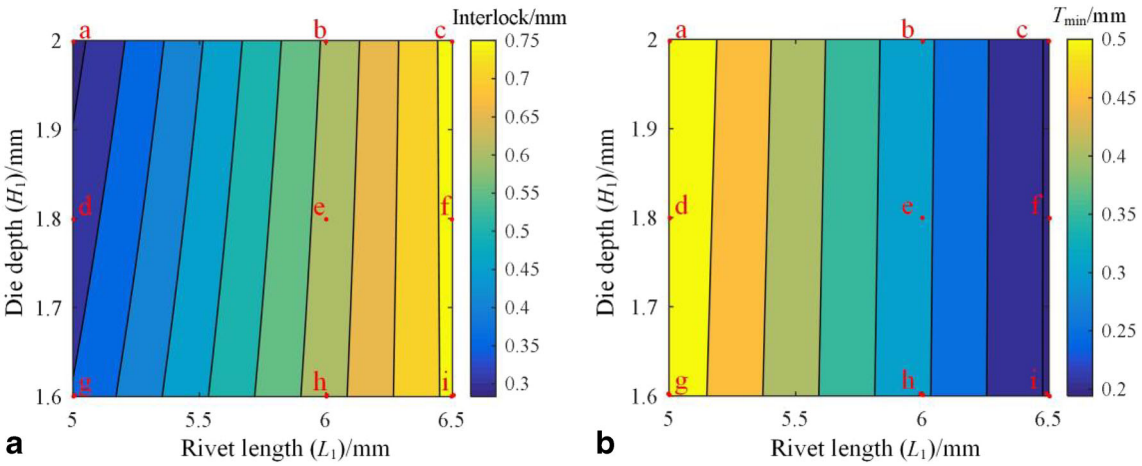

Fig. 17 Contour graphs of (a) the interlock and (b) the T_{min} with different rivet lengths and die depths (die diameter = 9.0 mm)

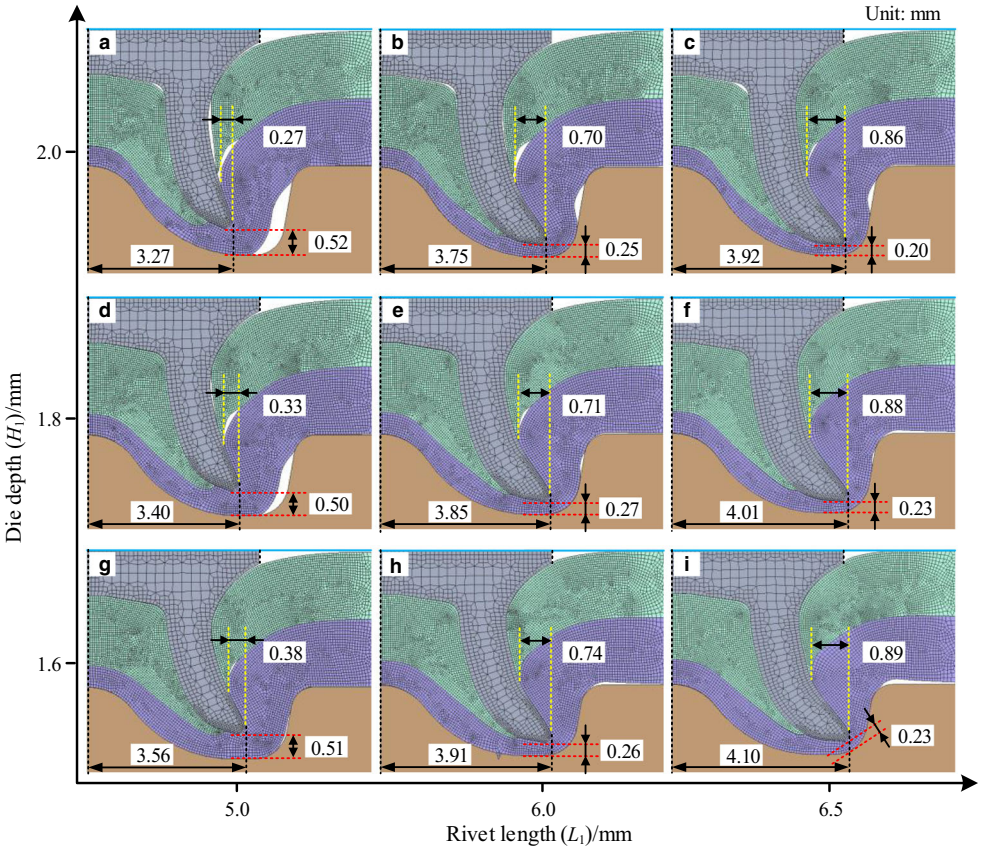

Fig. 18 Simulated joint cross-sectional profiles with different rivet lengths and die depths (D_1 = 9.0 mm) (**a**) L_1 = 5.0 mm, H_1 = 2.0 mm (**b**) L_1 = 6.0 mm, H_1 = 2.0 mm (**c**) L_1 = 6.5 mm, H_1 = 2.0 mm (**d**) L_1 = 5.0 mm, H_1 = 1.8 mm (**e**) L_1 = 6.0 mm, H_1 = 1.8 mm (**f**) L_1 = 6.5 mm, H_1 = 1.8 mm (**g**) L_1 = 5.0 mm, H_1 = 1.6 mm (**h**) L_1 = 6.0 mm, H_1 = 1.6 mm and (**i**) L_1 = 6.5 mm, H_1 = 1.6 mm

The simulated joint cross-sectional profiles at the points a~i in Fig. 19 are presented in Fig. 20. A good agreement between the predicted results from the developed regression models and the FEA simulation model was also found. For a given die diameter, the increase of the die depth was accompanied by the decreased interlock and the almost unchanged T_{min}. For a given die depth, the increased die diameter also lead to the decreased interlock and the almost constant T_{min}. It is worth mentioning that both of the interlock and the T_{min} varied within narrow ranges (i.e. 0.18 mm and 0.045 mm, respectively) in Fig. 19 than that in Fig. 13 or Fig. 17. This indicates the smaller influences of the die diameter and depth on the SPR joint quality than that of the rivet length under the studied joint configurations.

The relationship between the formation of the interlock and the die-to-rivet volume (R) was discussed

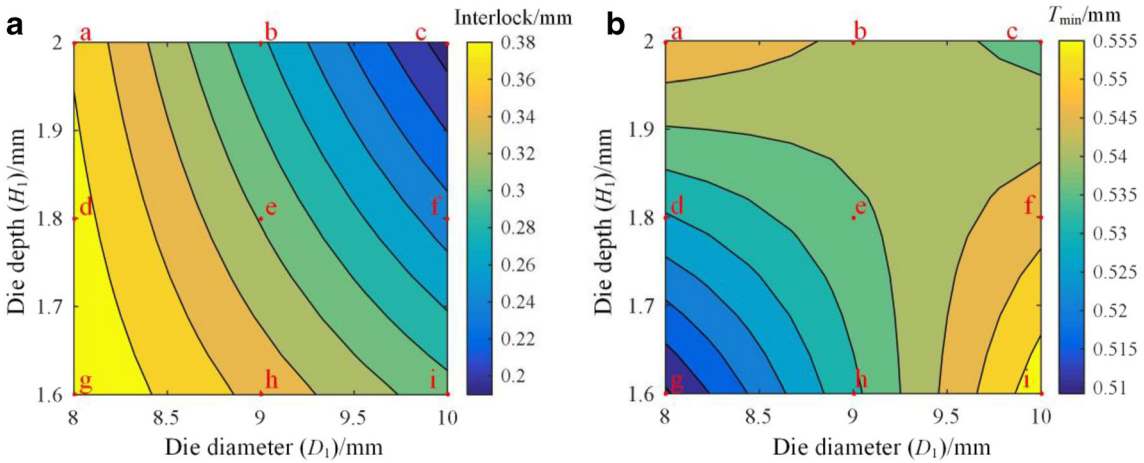

Fig. 19 Contour graphs of (a) the interlock and (b) the T_{min} with different die diameters and depths (rivet length = 5.0 mm)

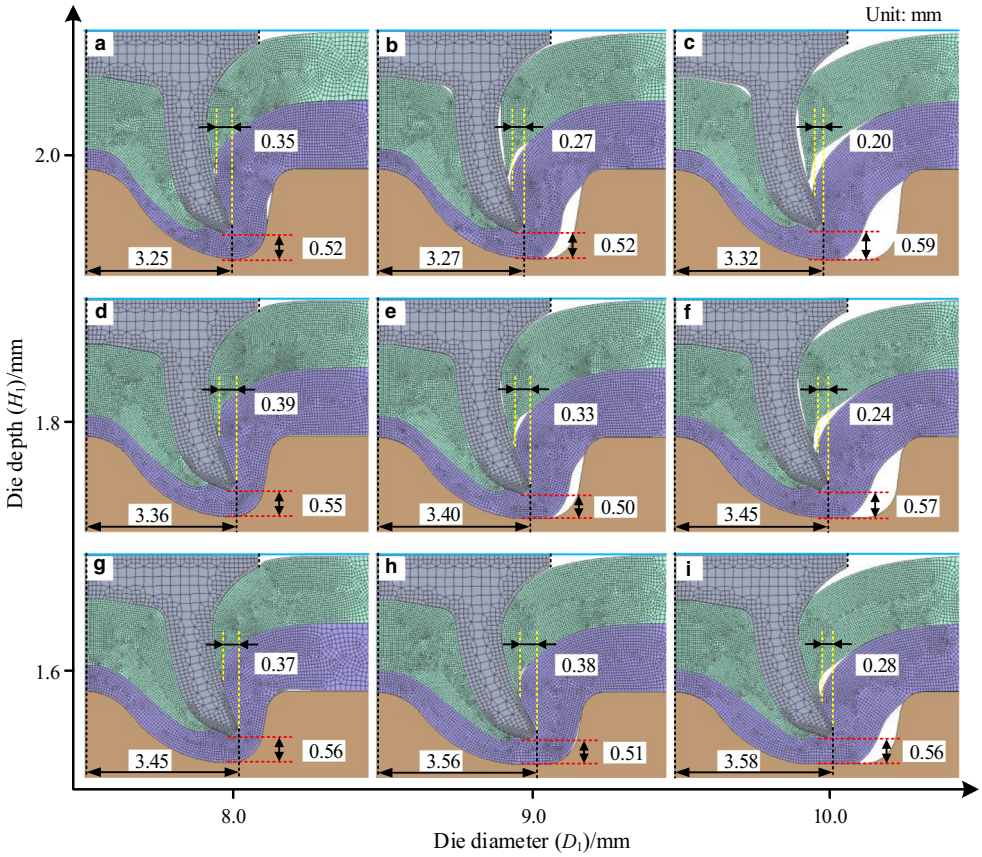

Fig. 20 Simulated joint cross-sectional profiles with different die diameters and die depths (L_1 = 5.0 mm) (**a**) D_1 = 8.0 mm, H_1 = 2.0 mm (**b**) D_1 = 9.0 mm, H_1 = 2.0 mm (**c**) D_1 = 10.0 mm, H_1 = 2.0 mm (**d**) D_1 = 8.0 mm, H_1 = 1.8 mm (**e**) D_1 = 9.0 mm, H_1 = 1.8 mm (**f**) D_1 = 10.0 mm, H_1 = 1.8 mm (**g**) D_1 = 8.0 mm, H_1 = 1.6 mm (**h**) D_1 = 9.0 mm, H_1 = 1.6 mm and (**i**) D_1 = 10.0 mm, H_1 = 1.6 mm

previously, hence here will not discuss further. It is worth mentioning that the maximum interlock was achieved on the lower left corner of the Fig. 19(a) with the R closer to 1.0, while the minimum interlock was observed on the upper right corner of the Fig. 19(a) when the R equals to 1.59. In addition, such interaction effect also revealed that when the R value is less than 1.0, the increment of the R value could lead to a larger interlock, but when the R value is greater than 1.0, the increment of the R value could result in a smaller interlock. Except for the R, the die depth is also very important because it directly determines when the rivet shank started flaring rapidly. Therefore, the die depth should be considered together with the R during the selection of rivet and die. For the studied material combination, the shallower die is better for the formation of the interlock. For other material combinations, further study is required.

5 Conclusions

In this study, simple but effective multiple regression models were proposed to predict the SPR joint quality. The interaction effects between the rivet and die parameters on the joint quality were graphically analysed and digitally validated. The main conclusions were listed as below:

1. The developed multiple regression models were proved effective to describe the relationships between the joining parameters and the SPR joint quality. The MAE values between the experimental results and regression predictions for the interlock and the T_{min} were 0.047 mm and 0.053 mm, respectively, and the corresponding MAPE were 10.4% and 12.3% under the studied joint configurations.
2. It is straightforward to analyse the interaction effects between the joining parameters on the joint quality by observing the contour graphs drawn from the developed regression models. Significant interaction effects between the rivet length, the die diameter and the die depth were identified on the interlock, but not on the T_{min} within the studied range.
3. By affecting the deformation behaviours of the rivets and sheets, the die-to-rivet volume ratio (R) significantly influenced the magnitude and changing trend of the interlock when with varying joining parameters. A larger interlock was more likely to be achieved when the R was close to 1.0.

The introduction of the regression model is the first step towards more complicated and more industrial applications by involving more joining parameters, such as the sheet thickness and the rivet hardness. In addition, it also offers the possibility to optimize the SPR joint quality by using the mathematic model together with other optimization algorithms.

Acknowledgements The authors would like to thank Dr. Matthias Wissling, Paul Bartig and their team members from Tucker GmbH for their supports during the laboratory tests.

Authors' contributions Huan Zhao, Li Han, Yunpeng Liu and Xianping Liu worked together to conceive this research. Huan Zhao designed the experiments, analysed the data and completed the original draft. Li Han supervised the experiments and provided critical paper revisions. Yunpeng Liu supported with the FEA simulation model and manuscript revision. Xianping Liu is the project leader and participated in the paper revision. All authors read and approved the final manuscript.

Funding This research is funded by Jaguar Land Rover Limited.

Data availability Not applicable

Compliance with ethical standards

Conflict of interest The authors declare that they have no conflict of interest.

Ethical approval Not applicable

Consent to participate Not applicable

Consent to publish Not applicable

References

1. Reinhert P (2004) The new Jaguar XJ - The first all aluminium car in monocoque design. Alum Int Today 16:21–24
2. Abe Y, Kato T, Mori K (2006) Joinability of aluminium alloy and mild steel sheets by self piercing rivet. J Mater Process Technol 177:417–421. https://doi.org/10.1016/j.jmatprotec.2006.04.029
3. He X, Zhao L, Deng C, Xing B, Gu F, Ball A (2015) Self-piercing riveting of similar and dissimilar metal sheets of aluminum alloy and copper alloy. Mater Des 65:923–933. https://doi.org/10.1016/J.MATDES.2014.10.002
4. Kotadia HR, Rahnama A, Sohn IR, Kim J, Sridhar S (2019) Performance of dissimilar metal self-piercing riveting (SPR) joint and coating behaviour under corrosive environment. J Manuf Process 39:259–270. https://doi.org/10.1016/J.JMAPRO.2019.02.024
5. Han L, Thornton M, Shergold M (2010) A comparison of the mechanical behaviour of self-piercing riveted and resistance spot welded aluminium sheets for the automotive industry. Mater Des 31:1457–1467. https://doi.org/10.1016/J.MATDES.2009.08.031
6. Li D, Chrysanthou A, Patel I, Williams G (2017) Self-piercing riveting-a review. Int J Adv Manuf Technol 92:1777–1824. https://doi.org/10.1007/s00170-017-0156-x
7. He X, Gu F, Ball A (2012) Recent development in finite element analysis of self-piercing riveted joints. Int J Adv Manuf Technol 58:643–649. https://doi.org/10.1007/s00170-011-3414-3
8. Haque R (2018) Quality of self-piercing riveting (SPR) joints from cross-sectional perspective: a review. Arch Civ Mech Eng 18:83–93. https://doi.org/10.1016/j.acme.2017.06.003
9. Kam DH, Jeong TE, Kim MG, Shin J (2019) Self-piercing riveted joint of vibration-damping steel and aluminum alloy. Appl Sci 9. https://doi.org/10.3390/app9214575
10. Zhang X, He X, Xing B, Wei W, Lu J (2020) Quasi-static and fatigue characteristics of self-piercing riveted joints in dissimilar aluminium-lithium alloy and titanium sheets. J Mater Res Technol. 9:5699–5711. https://doi.org/10.1016/j.jmrt.2020.03.095
11. Han L, Thornton M, Li D, Shergold M (2010) Effect of setting velocity on self-piercing riveting process and joint behaviour for automotive applications. SAE Tech Pap. https://doi.org/10.4271/2010-01-0966
12. Sun X, Khaleel MA (2005) Performance optimization of self-piercing rivets through analytical rivet strength estimation. J Manuf Process 7:83–93. https://doi.org/10.1016/S1526-6125(05)70085-2
13. Xu Y (2006) Effects of factors on physical attributes of self-piercing riveted joints. Sci Technol Weld Join 11:666–671. https://doi.org/10.1179/174329306X131866
14. Ma Y, Lou M, Li Y, Lin Z (2018) Effect of rivet and die on self-piercing rivetability of AA6061-T6 and mild steel CR4 of different gauges. J Mater Process Technol 251:282–294. https://doi.org/10.1016/J.JMATPROTEC.2017.08.020
15. Li DZ, Han L, Shergold M, Thornton M, Williams G (2013) Influence of rivet tip geometry on the joint quality and mechanical strengths of self-piercing riveted aluminium joints. Mater Sci Forum 765:746–750. https://doi.org/10.4028/www.scientific.net/MSF.765.746
16. Mucha J (2011) A study of quality parameters and behaviour of self-piercing riveted aluminium sheets with different joining conditions. Stroj Vestnik/Journal Mech Eng 57:323–333. https://doi.org/10.5545/sv-jme.2009.043
17. Han SL, Li ZY, Gao Y, Zeng QL (2014) Numerical study on die design parameters of self-pierce riveting process based on orthogonal test. J Shanghai Jiaotong Univ 19:308–312. https://doi.org/10.1007/s12204-014-1504-8
18. Jäckel M, Falk T, Landgrebe D (2016) Concept for further development of self-pierce riveting by using cyber physical systems. Procedia CIRP 44:293–297. https://doi.org/10.1016/j.procir.2016.02.073
19. Bhushan RK (2013) Optimization of cutting parameters for minimizing power consumption and maximizing tool life during machining of Al alloy SiC particle composites. J Clean Prod 39:242–254. https://doi.org/10.1016/j.jclepro.2012.08.008
20. Singh B, Ahuja N (2002) Development of controlled-release buccoadhesive hydrophilic matrices of diltiazem hydrochloride: Optimization of bioadhesion, dissolution, and diffusion parameters. Drug Dev Ind Pharm 28:431–442. https://doi.org/10.1081/DDC-120003004
21. Anawa EM, Olabi AG (2008) Using Taguchi method to optimize welding pool of dissimilar laser-welded components. Opt Laser Technol 40:379–388. https://doi.org/10.1016/j.optlastec.2007.07.001
22. Bitondo C, Prisco U, Squilace A, Buonadonna P, Dionoro G (2011) Friction-stir welding of AA 2198 butt joints: mechanical characterization of the process and of the welds through DOE analysis. Int J Adv Manuf Technol 53:505–516. https://doi.org/10.1007/s00170-010-2879-9
23. Zhao D, Wang Y, Liang D, Zhang P (2016) Modeling and process analysis of resistance spot welded DP600 joints based on regression

analysis. Mater Des. 110:676–684. https://doi.org/10.1016/j.matdes.2016.08.038

24. He X, Xing B, Zeng K, Gu F, Ball A (2013) Numerical and experimental investigations of self-piercing riveting. Int J Adv Manuf Technol 69:715–721. https://doi.org/10.1007/s00170-013-5072-0
25. Carandente M, Dashwood RJ, Masters IG, Han L (2016) Improvements in numerical simulation of the SPR process using a thermo-mechanical finite element analysis. J Mater Process Technol 236:148–161. https://doi.org/10.1016/J.JMATPROTEC.2016.05.001
26. Liu Y, Li H, Zhao H, Liu X (2019) Effects of the die parameters on the self-piercing riveting process. Int J Adv Manuf Technol 105:1–16. https://doi.org/10.1007/s00170-019-04567-4